LANGMUIR

Article

pubs.acs.org/Langmuir

Robust Maleimide-Functionalized Gold Surfaces and Nanoparticles Generated Using Custom-Designed Bidentate Adsorbates

Chul Soon Park, Han Ju Lee, Andrew C. Jamison, and T. Randall Lee*

Department of Chemistry and the Texas Center for Superconductivity, University of Houston, 4800 Calhoun Road, Houston, Texas 77204-5003, United States

Supporting Information

ABSTRACT: A series of custom-designed alkanethioacetate ligands were synthesized to provide a facile method of attaching maleimide-terminated adsorbates to gold nanostructures via thiolate bonds. Monolayers on flat gold substrates derived from both mono- and dithioacetates, with and without oligo(ethylene glycol) (OEG) moieties in their alkyl spacers, were characterized using X-ray photoelectron spectroscopy, polarization modulation infrared reflection−absorption spectroscopy, ellipsometry, and contact angle goniometry. For all adsorbates, the resulting monolayers revealed that a higher packing density and more homogeneous surface were generated when the film was formed in EtOH, but a higher percentage of bound thiolate was obtained in THF. A series of gold nanoparticles (AuNPs) capped with each adsorbate were prepared to explore how adsorbate structure influences aqueous colloidal stability under extreme conditions, as examined visually and spectroscopically. The AuNPs coated with adsorbates that include OEG moieties exhibited enhanced stability under high salt concentration, and AuNPs capped with dithioacetate adsorbates exhibited improved stability against ligand exchange in competition with dithiothreitol (DTT). Overall, the best results were obtained with a chelating dithioacetate adsorbate that included OEG moieties in its alkyl spacer, imparting improved stability via enhanced solubility in water and superior adsorbate attachment owing to the chelate effect.

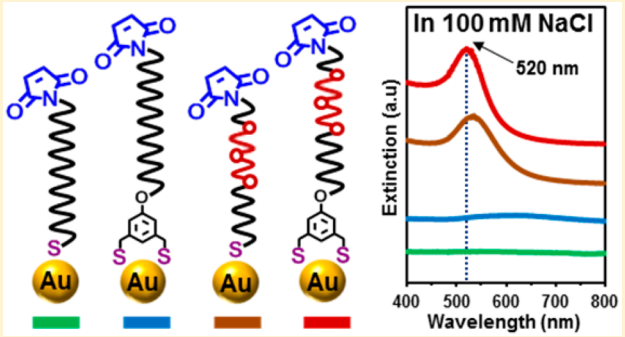

INTRODUCTION

Self-assembled monolayers (SAMs) are thin films spontaneously formed typically from amphiphilic molecules on substrates such as metal, metal oxide, and semiconductor surfaces.[1,2] In particular, SAMs derived from the interaction of sulfur and gold have been extensively investigated because of the great affinity between them as well as the ease of generation and characterization of these monolayers. Thiolate SAMs can be prepared from adsorbates with thiol and disulfide as well as thioacetate headgroups.[3−5] And it is remarkably easy to control the interfacial properties of the resulting films by varying the nature of the terminal functional groups (tailgroups).[1,7,8] For research involving the attachment of biomolecules to surfaces, the terminal groups used have included carboxylic acid,[6] amine,[7] and maleimide groups[9] exposed at the interface. The maleimide group is an especially fascinating attachment moiety that can make highly efficient and stable linkages. The coupling between maleimide and cysteine thiols based on the Michael addition reaction is one of the most well-known and commonly utilized bioconjugation techniques for labeling DNA, proteins, and peptides because maleimide is a highly reactive Michael acceptor.[10] In addition, this coupling reaction has little or no effect on the biological activity of the targeted biomolecule. This strategy has therefore been used to conjugate thiol-reactive polymers with peptides and proteins[11,12] and applied to SAMs generated for attaching peptides and carbohydrates onto gold surfaces.[9,13] Additionally, this coupling strategy has also been employed with inorganic and polymeric nanoparticles.[14,15]

To form maleimide-functionalized gold surfaces and gold nanoparticles (AuNPs) from maleimide-bearing thiol-based adsorbates, many studies have first protected the maleimide group of the adsorbate from possible intermolecular reactions by forming a Diels−Alder product. After attachment to the surface, the protected maleimide group is then deprotected using a retro-Diels−Alder reaction.[16,17] An example would be the furan-protected maleimide−thiol utilized by Zhu et al. to modify the surfaces of AuNPs. After deprotection, the authors attached a thiol-terminated ^{18}F-labeled compound for biological studies. However, this strategy requires an elevated temperature of around 95 °C to initiate the retro-Diels−Alder reaction, a temperature that can lead to the detachment of the frequently used monodentate thiolates from gold surfaces. It has been shown that monolayers derived from monodentate adsorbates are markedly less stable than those generated from bidentate adsorbates on both flat gold surfaces and AuNPs.[6,7,18]

Received: April 5, 2016
Revised: June 30, 2016
Published: July 6, 2016

DOI: 10.1021/acs.langmuir.6b01299
Langmuir 2016, 32, 7306−7315

An alternative strategy for enabling surface attachment of bulky groups involves the use of click reactions,[19,20] which offer a simple and facile strategy to functionalize gold surfaces. These reactions, however, typically require the use of a copper catalyst, which can have deleterious effects on biological systems through Fenton reactions.[21] To prevent this drawback, copper-free click reactions have been studied that utilize highly strained cyclooctynes, yet these compounds can be difficult to synthesize.[22,23] To overcome these collective concerns, we describe in this report the design and synthesis of a series of robust maleimide-terminated adsorbates that pair the maleimide moiety with a thioacetate headgroup. Additionally, for AuNPs, which are colloidally unstable in organic solvents or aqueous environments without surface ligands, we chose to test two types of structural assemblies to evaluate which would work best to prevent aggregation in aqueous solution. The choice of stabilizing ligand is especially important when the targeted application for the adsorbate-modified AuNPs involves biological contact. From this perspective, oligo(ethylene glycol)-terminated ligands have proven to be effective because they offer good colloidal stability in aqueous systems and low conjugate toxicity.[24]

For the present study, we prepared four custom-designed adsorbates with the goal of enhancing SAM formation and stability for AuNP systems bearing maleimide-terminated ligands, which will allow further modification of the AuNP surfaces. First, we sought to prevent the coupling between the thiol termini of our adsorbates and the maleimide moiety by using a thioacetate rather than thiol headgroup. Second, our strategy to prepare maleimide-terminated AuNPs for facile attachment of biomolecules avoids the use of toxic metal catalysts, producing AuNPs with greater biocompatibility than those prepared using copper-catalyzed click reactions. Third, we anticipated that AuNPs decorated with adsorbates containing an oligo(ethylene glycol) (OEG) unit in their spacer would enhance colloidal stability, not only in aqueous solution but also in saline. Finally, we also anticipated that AuNPs capped with bidentate adsorbates would exhibit enhanced stability against ligand exchange owing to the chelate effect. The complete set of custom-designed maleimide-terminated alkanethioacetate prepared for this report is shown in Figure 1.

The two maleimide-terminated adsorbates having a simple alkyl spacer are the monothiol *S*-(15-(2,5-dioxo-2,5-dihydro-1*H*-pyrrol-1-yl)pentadecyl)ethanethioate (MM) and the bidentate dithiol *S*,*S*′-((5-((15-(2,5-dioxo-2,5-dihydro-1*H*-pyrrol-1-yl)pentadecyl)oxy)-1,3-phenylene)bis(methylene))diethanethioate (BM). Two comparable adsorbates having oxyethylene moieties in their alkyl spacer were also prepared: the monothiol *S*-(6-(2-(2-(2-(2,5-dioxo-2,5-dihydro-1*H*-pyrrol-1-yl)ethoxy)ethoxy)ethoxy)hexyl)ethanethioate (MEM) and the bidentate dithiol *S*,*S*′-((5-((6-(2-(2-(2-(2,5-dioxo-2,5-dihydro-1*H*-pyrrol-1-yl)ethoxy)ethoxy)ethoxy)hexyl)oxy)-1,3-phen-ylene)bis-(methylene))diethanethioate (BEM). Additionally, a reference SAM was prepared from octadecanethiol (C18SH).

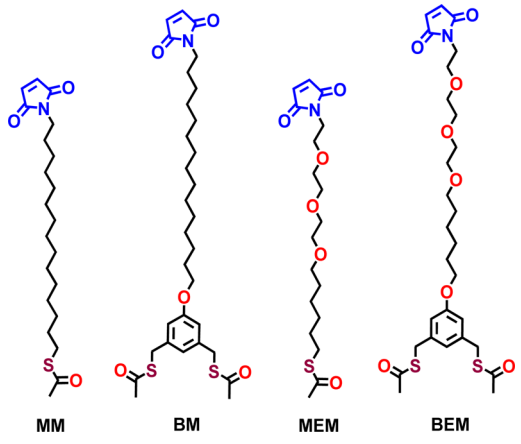

Figure 1. Structures of maleimide-terminated alkanethioacetate examined in this study.

EXPERIMENTAL SECTION

Information regarding the materials, procedures, and instrumental methods used to perform the research reported herein is provided in the Supporting Information, which also contains ^{1}H and ^{13}C NMR spectra for all custom-designed adsorbates (MM, BM, MEM, and BEM; see Figures S1–S8).

RESULTS AND DISCUSSION

Characterization of SAMs Derived from Maleimide-Terminated Adsorbates on Flat Gold Surfaces. To evaluate the efficiency of two common deposition solvents at forming the new SAMs, evaporated gold slides were immersed in ethanolic (EtOH) and tetrahydrofuran (THF) solutions in vials prepared for each of the adsorbate/solvent combinations. These slides were incubated for at least 48 h at rt to allow sufficient time for the solution/substrate systems to equilibrate. The resultant SAM-coated gold slides were then characterized by X-ray photoelectron spectroscopy (XPS), ellipsometry, polarization-modulation infrared reflection–absorption spectroscopy (PM-IRRAS), and contact angle goniometry. The corresponding SAM-coated gold nanoparticles (~15 nm diameter) were examined by UV–vis spectroscopy.

X-ray Photoelectron Spectroscopy. X-ray photoelectron spectra provide vital information for the characterization of self-assembled monolayers. The most fundamental detail for these films, the elemental composition, can be confirmed by the position and intensity of the spectral peaks. For thiolate adsorbates, the binding energies (BEs) of the sulfur atoms can be used to evaluate the nature and degree of bonding between the headgroups and gold, while the BE peak areas for the S 2p orbitals can be used to calculate the relative packing densities of the adsorbates in these films, provided steps are taken to ameliorate fluctuations in the intensity of the signals. Therefore, for our XPS analyses, the Au 4f BE was used, not only to reference the BE scales for the spectra but also to generate S/Au ratios to calculate packing densities. The X-ray photoelectron spectra for the Au 4f region are shown in Figure S9 and are consistent with those found in the literature.[6]

Figure 2 shows the spectra for all elements other than gold in the SAMs formed from the thioacetates (and C18SH) prepared for this study. A prior report by our research group found that thioacetates experience a loss of the acetyl group during SAM formation, affording monolayer films with diminished conformational order and packing density when compared to analogous thiol-derived SAMs.[5] Given this prior study, we anticipated that the S 2p spectra for the resulting films would resemble those of SAMs formed from alkanethiols. Studies have shown that the S $2p_{3/2}$ and S $2p_{1/2}$ BE peaks appear at ~162.0 and ~163.2 eV, respectively, for bound thiolate sulfur.[25] Unbound thioacetate, thiol, and disulfide species show peaks in the range of ~163–166 eV, and oxidized sulfur species show

DOI: 10.1021/acs.langmuir.6b01299
Langmuir 2016, 32, 7306–7315

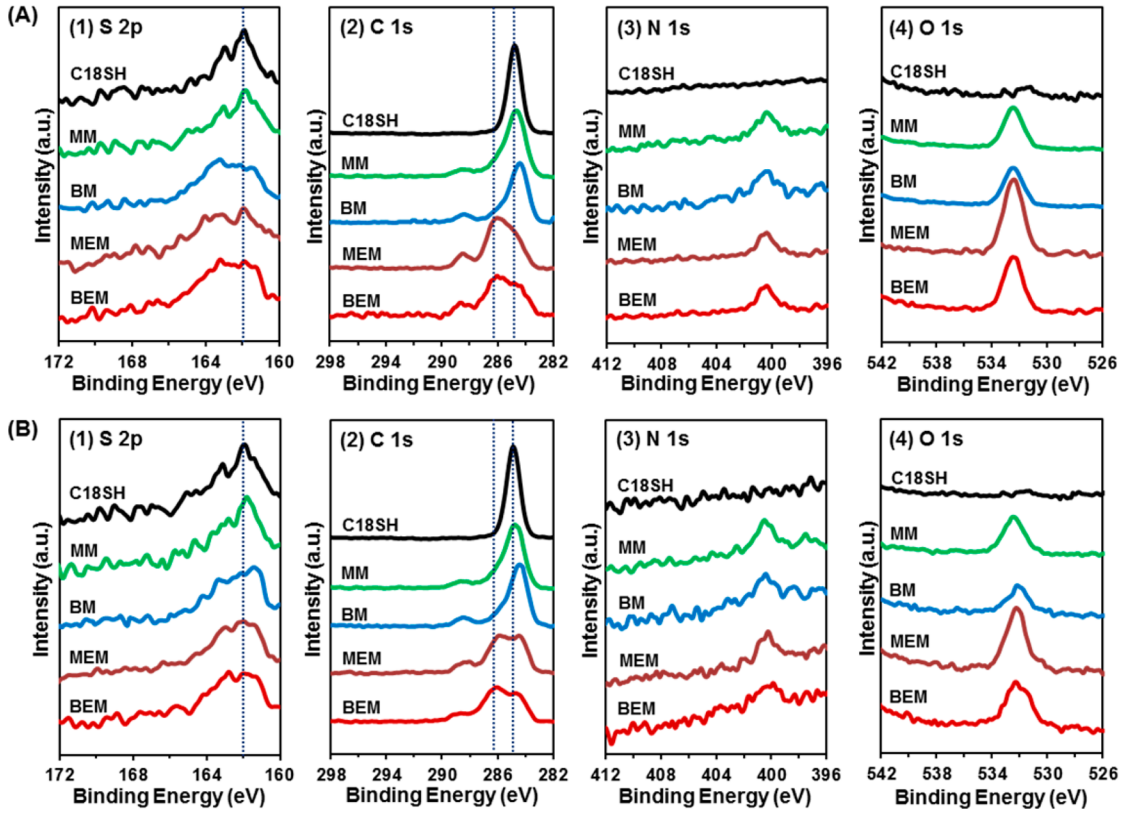

Figure 2. X-ray photoelectron spectra of the SAMs derived from the maleimide-terminated alkanethioacetate as compared to that from C18SH for the (1) S 2p, (2) C 1s, (3) N 1s, and (4) O 1s spectral regions for SAMs formed in (A) EtOH or (B) THF.

peaks at ~169 eV.[26−28] In plot 1 of Figures 2A and 2B, no oxidized sulfur species are observed at ~169 eV for all SAMs prepared in this study using both solvent systems (EtOH and THF). Peak fitting of the S 2p peaks to resolve bound thiolate versus unbound thioacetate species reveals that THF is a more effective solvent than EtOH for preparing SAMs from these new adsorbates (see Figure S10), with all four thioacetate-derived SAMs producing higher percentages of bound thiolate in THF. But this higher percentage failed to translate into higher packing densities for the adsorbates in the monolayer, as noted in Table 1. To derive the relative packing densities, we used the C18SH SAM as a reference system and considered its adsorbate surface coverage to be 100%, using S/Au ratios to conduct the calculations; this procedure is described in detail in the Supporting Information. The data reveal that all four thioacetate-derived SAMs prepared in EtOH have higher packing densities than those prepared in THF, which is consistent with studies of SAM growth in a previous report.[7] Furthermore, the dithioacetate-derived SAMs prepared in EtOH exhibited maximal packing densities, given that the bidentate adsorbates (BM and BEM) afford SAMs with an equivalent number of S−Au bonds as the C18SH reference SAM (i.e., both bidentate SAMs exhibit ~50% packing density).

For the C 1s region, there are significant differences in the spectra of the various alkanethioacetate-generated SAMs, as shown in plot 2 of Figures 2A and 2B. The C 1s BE peak positions for the methylene carbons of the extended alkyl chain appear at ~284.8, ~284.6, and ~284.4 eV for the SAMs formed from C18SH, MM, and BM in EtOH, respectively (i.e., for the SAMs formed from the adsorbates with no OEG linkages). In contrast, the C 1s BE peaks appear at ~284.7, ~284.4, and ~284.2 eV for the C18SH, MM, and BM SAMs formed in THF, respectively. In both solvents, the BEs of the C 1s carbons shift to slightly lower energies for the BM SAMs (bidentate adsorbates) as compared to the MM SAMs (monodentate adsorbates) by ~0.2 eV and also for the MM SAMs as compared to the C18SH SAMs. Furthermore, this peak for the SAMs derived from BM and MM is broader than that from C18SH in both solvents. These small differences in C 1s binding energy are related to the relative coverage of the

Table 1. Ellipsometric Thicknesses, Relative Packing Densities, and Percentages of Bound Thiolate for SAMs Derived from C18SH, MM, BM, MEM, and BEM in EtOH and THF

	ellipsometric thickness (Å)		relative adsorbate packing density[a] (%)		percentage of bound thiolate[b] (%)	
adsorbate	EtOH	THF	EtOH	THF	EtOH	THF
C18SH	22.7 ± 0.7	22.0 ± 0.3	100	100	99	99
MM	20.1 ± 0.8	17.4 ± 0.4	84	83	87	92
BM	20.3 ± 0.6	17.9 ± 0.6	49	43	77	81
MEM	20.2 ± 0.1	16.7 ± 0.8	82	80	85	90
BEM	18.8 ± 0.4	15.8 ± 0.5	47	42	80	82

[a]Prior studies determined that the reproducibility of our adsorbate packing densities using our XPS instrument and the same data collection protocols fell within ±2%.[29] For the relative packing densities, the C18SH SAM was assumed to be 100% for making comparisons with the packing densities of the monolayers derived from other adsorbates. [b]Percentages of bound thiolate were obtained from the deconvoluted S 2p spectra. The S/Au ratios for BM and BEM were divided by a factor of 2 to compare with the data for the monodentate adsorbates.

DOI: 10.1021/acs.langmuir.6b01299
Langmuir 2016, 32, 7306−7315

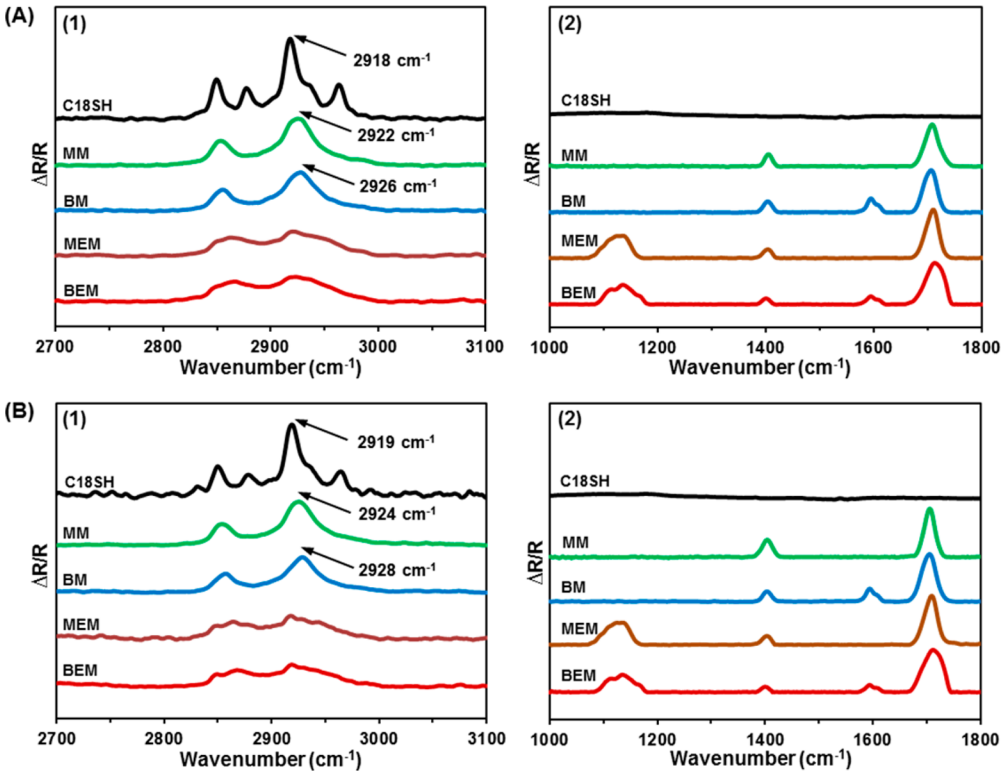

Figure 3. PM-IRRAS spectra of (1) the C−H stretching region and (2) the region from 1050 to 1850 cm^{-1} for the SAMs derived from C18SH, MM, BM, MEM, and BEM prepared in (A) EtOH and (B) THF.

adsorbates on the substrates and the associated packing characteristics.[30] With regard to the shift in BE to lower energy, similar trends have been interpreted to arise from the fact that an emitted C 1s electron can be easily replaced in a loosely packed assembly of chains because well-packed alkyl chain assemblies act as good insulators.[31] Based on these results, more densely packed monolayers appear to be forming in EtOH than in THF.

The X-ray photoelectron spectra can also be used to confirm the presence of key structural components within the monolayer films. The SAMs derived from MEM and BEM exhibit an additional C 1s peak at ∼286 eV that reflects the presence of the carbons of the ether linkages (C−O−C).[32] Additionally, a minor peak at ∼288.5 eV can be seen in the spectra for all of the thioacetate-derived SAMs, which can be attributed to the carbonyl carbons of the maleimide moieties.[33] The maleimide tailgroups also generate an N 1s peak at ∼400 eV, as shown in plot 3 of Figures 2A and 2B.[33] These features in the X-ray photoelectron spectra appear to confirm the presence of the maleimide tailgroups for all four SAMs. The O 1s peaks at ∼532 eV in plot 4 of Figures 2A and 2B exhibit notable differences between the various monolayers; the intensities are greater for the monolayers derived from MEM and BEM, indicating a higher oxygen content as compared to the SAMs formed from MM and BM. These results can be rationalized by the fact that MEM and BEM contain OEG groups in their alkyl spacers.[34,35] Furthermore, even though BEM possesses more oxygen atoms than MEM in its tailgroup, it exhibits a less intense O 1s peak—a consequence of the reduced packing density for this SAM.

Ellipsometry. Table 1 provides the ellipsometric film thickness data for the SAMs prepared in both EtOH and THF. The average thicknesses of the monolayers derived from C18SH in EtOH is 23 Å and for THF is 22 Å—values that are consistent with the literature.[7,36] For all SAMs prepared in THF, the thicknesses of the SAMs were noticeably less than those assembled in EtOH, which is plausibly related to a lower packing density for these films, as also indicated by the XPS data. For the monolayers formed in each of the deposition solvents, the four SAMs have film thicknesses that are statistically equivalent, a result that fails to align with the differences that would be anticipated from the inclusion of the aromatic moiety in two of the four adsorbate structures. Lee et al. also found a statistical equivalence for film thicknesses of a similarly structured set of SAMs derived from monothiolate and dithiolate adsorbates.[6] These results were rationalized by the fact that the bidentate adsorbate produced a monolayer with a reduced number of molecules on the gold surface, creating a situation where the increase in space between the surface chains was offset by an increase in the tilt of these chains as they are drawn together by van der Waals forces. Surprisingly, the SAMs incorporating the OEG moieties in the surface chains (i.e., the films derived from MEM and BEM) afforded thickness results similar to those of the SAMs with unmodified alkyl spacers (i.e., the films derived from MM and BM). Harder et al. have explained this circumstance by showing that differences can exist in the conformational order for SAMS with OEG-terminated chains, and that such chains can adopt an *all-trans* alignment that is enforced by the packing of the SAM assembly, as contrasted with the less ordered helical OEG conformation.[34]

Polarization Modulation Infrared Reflection−Absorption Spectroscopy. Surface infrared spectra enable a conformational analysis of the collective extended alkyl chains of adsorbates (when such chains are present) and characterization of the functional groups within the film.[37] With regard to the

DOI: 10.1021/acs.langmuir.6b01299
Langmuir 2016, 32, 7306−7315

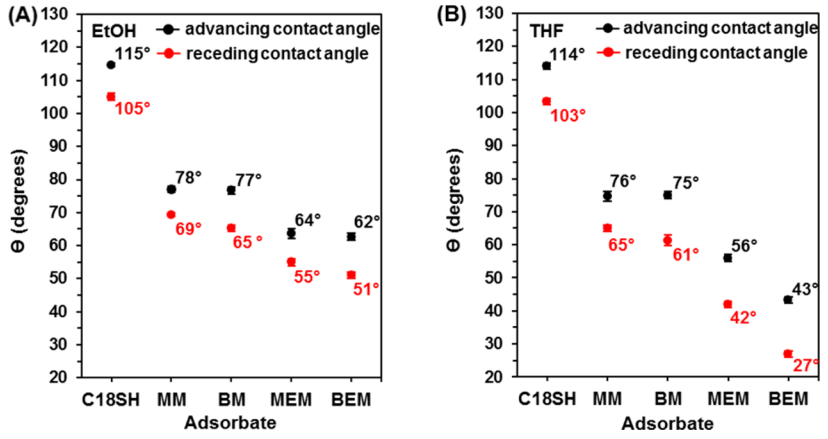

Figure 4. Advancing and receding contact angles of SAMs generated from C18SH, MM, BM, MEM, and BEM prepared in (A) EtOH and (B) THF.

alignment of the methylene units of the alkyl chains, the degree of order for the adsorbates of a SAM has frequently been evaluated using the peak positions of the C−H vibrations within the PM-IRRAS spectrum. When the carbons in an alkyl chain adopt an *all-trans* alignment (a low-energy conformation), the band associated with the antisymmetric methylene C−H stretching vibration ($\nu_a^{CH_2}$) shifts to ∼2918 cm^{-1}.[6,7] Therefore, this band position has been interpreted to indicate that the chains are mostly immobile, and that the assembly is crystalline. In contrast, a $\nu_a^{CH_2}$ band position of ∼2924 cm^{-1} has been associated with alkyl chains that contain a significant number of gauche alignments (a higher energy conformation), and the chains are more disordered and liquidlike in comparison. A similar analysis using $\nu_s^{CH_2}$ can also be performed.

Plot 1 of Figures 3A and 3B provides the spectra for the SAMs derived from C18SH, MM, BM, MEM, and BEM. The band positions of $\nu_a^{CH_2}$ for the SAMs containing alkyl chain segments of 15 methylenes or more (C18SH, MM, and BM) gave rise to $\nu_a^{CH_2}$ positions at 2918, 2922, and 2926 cm^{-1} when prepared in EtOH as well as at 2919, 2924, and 2928 cm^{-1} when prepared in THF, each, respectively. According to these results, the relative conformational order for the adsorbate chains in these SAMs is as follows: C18SH > MM > BM.[6] SAMs formed in EtOH show a greater degree of order than those prepared in THF, which is consistent with the packing densities derived from the XPS data. Unfortunately, the intensities of the $\nu_a^{CH_2}$ bands associated with the shorter alkyl chain segments (six methylenes) of the SAMs derived with MEM and BEM are insufficiently strong to allow direct comparison with the other SAMs or to distinguish them from the peaks associated with other methylene moieties present in these monolayers. Additionally, all of the new adsorbates show a strong C═O stretching vibration associated with the imide carbonyl of the maleimide moieties at ∼1708 cm^{-1}, as shown in plot 2 of Figures 3A and 3B.[33] Further, we observe stretching vibrations for C−O−C of the OEG moieties of MEM and BEM at ∼1130 cm^{-1} and the aromatic C═C bonds for BM and BEM at ∼1600 cm^{-1} in plot 2 of Figures 3A and 3B.[38−40] Additionally, the symmetric C−N−C stretch for the maleimide moieties appears at ∼1405 cm^{-1} for all of the thioacetate-derived monolayers. For the SAM formed from C18SH, the IR modes in these latter regions were too weak when the spectrum was displayed at the same scale as the functionalized SAMs.

Contact Angle Measurements. Contact angle goniometry is a useful method to analyze the interfacial properties and the chemical nature and structure of the tailgroups of SAMs. The advancing contact angle (θ_a) and receding contact angle (θ_r) for water on the SAMs prepared both in EtOH and THF are shown in Figure 4. Contact angle hysteresis ($\Delta\theta = \theta_a - \theta_r$) also provides insight into the interfacial properties, especially the relative roughness or heterogeneity of the interface. Figure 4A shows the advancing and receding contact angles for water for the SAMs derived from C18SH, MM, BM, MEM, and BEM prepared in EtOH; the averages of the measurements were 115°, 78°, 77°, 64°, and 62°, respectively. For the SAM formed from C18SH, the value of 115° is consistent with that found in the literature.[41] The value of θ_a for water on SAMs derived from MM also compares well with that found in the literature for a maleimide-terminated film.[42] For SAMs derived from MM and BM in EtOH, the advancing contact angle for water was ∼14° higher than the SAMs formed from MEM and BEM in EtOH, a difference that can be rationalized by the fact that the MEM and BEM adsorbates include hydrophilic tri(ethylene glycol)-derived chain segments just below the maleimide moiety. This increased wetting for the MEM and BEM SAMs is similarly observed in the data for the SAMs prepared from THF (Figure 4B); however, the contact angles for the latter show lower values when compared to the SAMs generated in EtOH, plausibly because the SAMs prepared in THF are less-ordered than the SAMs prepared in EtOH. With regard to $\Delta\theta$, large hysteretic values can be interpreted to indicate that the contacting liquid intercalates into the film—a sign of either surface roughness and/or interfacial disorder. The hysteresis for SAMs derived from C18SH is ∼10°, which is consistent with that of alkanethiol-derived SAMs in the literature.[41] The hystereses for SAMs derived from MM, BM, MEM, and BEM are 9°, 12°, 9°, and 11° when formed in EtOH and 11°, 14°, 14°, and 16° when prepared in THF. The hystereses for the SAMs prepared in EtOH exhibit relatively low values that are similar to that obtained for the well-packed and well-ordered C18SH SAM. Accordingly, it is reasonable to conclude from the contact angle results that the surfaces of the SAMs prepared in EtOH present an interface that is better ordered than the SAMs prepared in THF.

Verification of Terminal Maleimide Species in the Films: Exposure to Hexachlorocyclopentadiene (HCCPD). To verify that the maleimide tailgroups retain their chemical activity once attached to the gold surfaces, we conducted a Diels−Alder reaction between the MM SAMs and hexachlorocyclopentadiene (HCCPD; see the Supporting Information for additional details).[43] Before conducting the

DOI: 10.1021/acs.langmuir.6b01299
Langmuir 2016, 32, 7306−7315

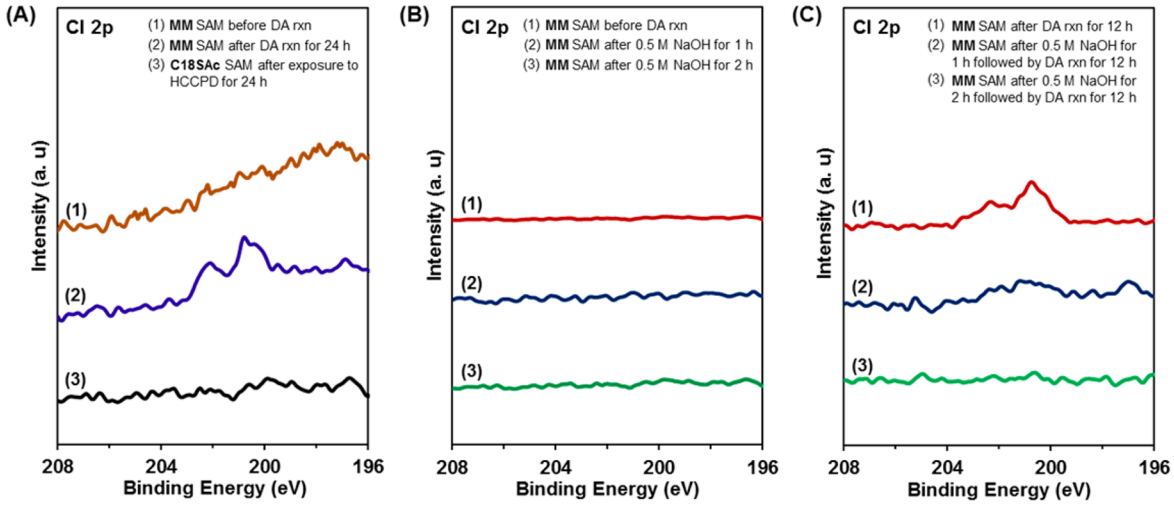

Figure 5. X-ray photoelectron spectra of the Cl 2p spectral region for (A-1) MM SAM before exposure to HCCPD, (A-2) MM SAM after exposure to HCCPD for 24 h, (A-3) C18SAc SAM after exposure to HCCPD for 24 h, (B-1) MM SAM before exposure to HCCPD, (B-2) MM SAM treated with 0.5 M NaOH for 1 h, (B-3) MM SAM treated with 0.5 M NaOH for 2 h, (C-1) MM SAM after exposure to HCCPD for 12 h, (C-2) MM SAM treated with 0.5 M NaOH for 1 h followed by exposure to HCCPD for 12 h, and (C-3) MM SAM treated with 0.5 M NaOH for 2 h followed by exposure to HCCPD for 12 h.

Diels–Alder reaction, the initial MM film thickness for the SAM prepared for this experiment was ~19 Å. Notably, the film thickness for the SAM increased ~4 Å after exposure to the 3.6 mM HCCPD solution for 24 h (see Table S5), verifying that the maleimide reactive site (the alkene bond) remained intact after film formation. As further verification of the successful formation of the Diels–Alder adduct, we collected XPS spectra for the MM SAM before and after exposure to the HCCPD solution for 24 h. In spectrum 1 of Figure 5A, there are no peaks for Cl 2p in the XPS spectrum collected before the Diels–Alder reaction; however, Cl 2p peaks appear in the spectrum collected after the Diels–Alder reaction (spectrum 2 in Figure 5A). In a control experiment, we similarly treated of the alkyl-terminated SAM formed from octadecanethioacetate (C18SAc) with HCCPD, which showed no peaks for Cl 2p (spectrum 3 in Figure 5A).

Furthermore, to verify that the Diels–Alder reaction detected by spectrum 2 of Figure 5A occurred between HCCPD and maleimide rather than a partially hydrolyzed derivative of latter, we subjected the MM SAMs to conditions that are known to effect partial hydrolysis of such five-membered ring systems.[44] The spectra in Figure 5B demonstrate the absence of chlorine in the SAMs prior to any Diels–Alder reaction with HCCPD. In contrast, spectrum 1 in Figure 5C shows substantial incorporation of chlorine after treatment with HCCPD solution for 12 h. Notably, spectrum 2 in Figure 5C shows that the partially hydrolyzed SAM was markedly less reactive toward HCCPD, and further hydrolysis gives a surface that is nonreactive toward HCCPD (spectrum 3 in Figure 5c). On the basis of these collective data, we conclude that the maleimide moieties successfully react with HCCPD via Diels–Alder reaction and are thus chemically viable in the films.

Colloidal Stability Tests: Exposure to Solutions Containing High Ion Content or a Reducing/Displacing Reagent. Our analysis of the SAMs formed on flat gold from the series of new maleimide-terminated thioacetates suggests that these adsorbates are suitable for forming well-ordered coatings on gold nanoparticles. Achieving long-term colloidal stability for such nanoparticles is also necessary for the development of nanoprobes for biological conditions. Therefore, we performed colloidal stability tests on AuNPs capped with each of the new adsorbates in the presence of various concentrations of NaCl and dithiothreitol (DTT). The AuNPs dispersed in a solvent can be characterized by UV–vis spectroscopy, as demonstrated previously.[45] For such studies, the particle size, stabilizer, and surrounding medium each influence the surface plasmon resonance (SPR) bands of the AuNPs.[46] Furthermore, in cases where the gold nanoparticles aggregate and ultimately precipitate, red-shifting, peak broadening, and a reduction of the intensity of the SPR bands are commonly observed.[47] For our experimental work, we initially prepared citrate-stabilized AuNPs that were ~15 nm in diameter, producing the red-hued solution shown in Figure 6A; the preparation of the AuNPs is detailed in the Supporting Information. After displacement of citrate with thioacetate, the solutions with the AuNPs capped with MM and BM exhibited a change in color, producing a slight purple tint, while the AuNPs capped with MEM and BEM retained almost the same color as the citrate-stabilized AuNPs. To compare the stability in aqueous solution of the AuNPs capped with each of the adsorbates, we measured the extinction spectra for each of the AuNPs capped with MM, BM, MEM, and BEM as well as the citrate-stabilized AuNPs as a control sample. As shown in Figure 6B, the ~15 nm citrate-stabilized AuNPs show a maximum peak intensity at 520 nm. However, the AuNPs capped with MM and BM showed significant red-shifts to 530 and 527 nm, respectively. These results can be compared to those obtained with the AuNPs coated with MEM, which exhibited a smaller red-shift at 524 nm. However, the position of the SPR peak for the AuNPs capped with BEM was located at 520 nm, which is the same as the citrate-stabilized AuNPs. According to these results, we conclude that the AuNPs capped with adsorbates containing OEG moieties (BM and BEM) appear to exhibit enhanced aggregation resistance compared to MM because they impart good solubility characteristics to the particles in water, while the bidentate-capped AuNPs (coated with MEM and BEM) appear to be effective at stabilizing the AuNPs by resisting desorption and/or displacement.[17,48]

DOI: 10.1021/acs.langmuir.6b01299
Langmuir 2016, 32, 7306–7315

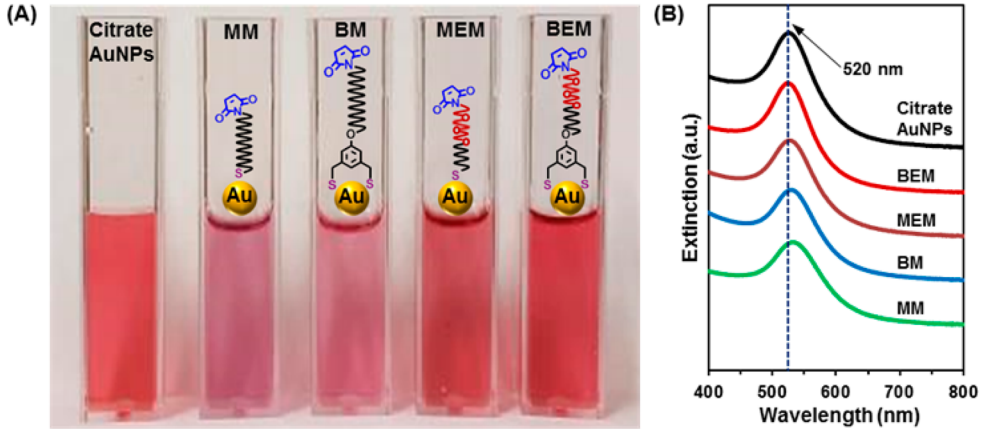

Figure 6. (A) Images of AuNP solutions where the ~15 nm AuNPs have been stabilized with either citrate, MM, BM, MEM, or BEM. (B) UV–vis spectra of the same AuNP solutions where the ~15 nm AuNPs have been stabilized with either citrate, MM, BM, MEM, or BEM.

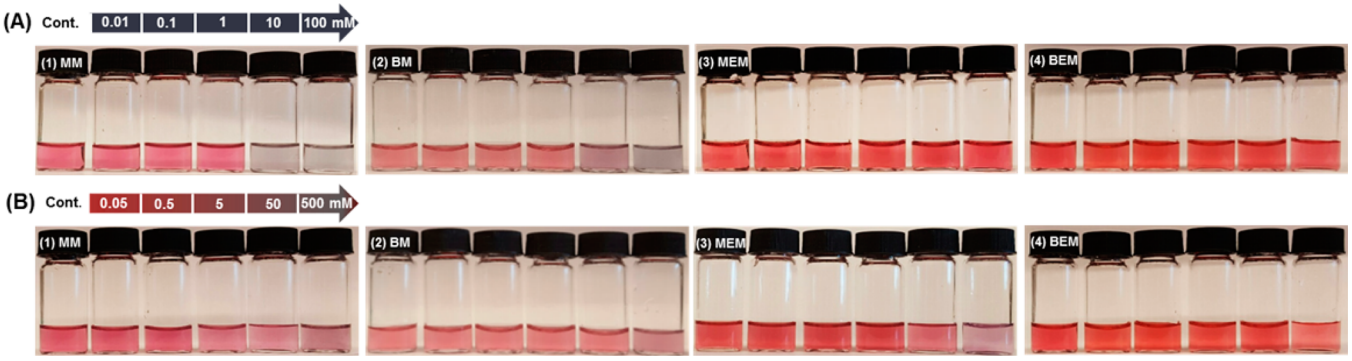

Figure 7. Images of aqueous solutions containing ~15 nm AuNPs capped with MM, BM, MEM, or BEM after 48 h for (A) the NaCl stability test and (B) the DTT stability test. (Controls are the AuNPs capped with each of the adsorbates without NaCl or DTT present.)

Our initial analysis of the stability of our AuNP systems using UV–vis spectroscopy is tempered by the knowledge that the shift in the extinction (SPR) band can be influenced by the adsorbate coating in contact with the gold nanoparticle surface.[49] Therefore, we examined the long-term colloidal stability of the AuNPs under extreme conditions such as high ionic content in the solution (NaCl) and high concentrations of a reducing/displacing reagent (DTT).[50] High ionic conditions can influence the solubility of AuNPs in two possible ways. First, for citrate-stabilized AuNPs, which are electrostatically stabilized, the Debye screening length will be reduced by adding salt, which will encourage aggregation. Ligand-capped AuNPs can also aggregate owing to a reduction in electrostatic repulsive forces between particles. Second, high ionic conditions can change the solubility of the adsorbates that are bound to the AuNPs, providing another means of promoting aggregation. For our series of AuNPs, the added NaCl increases the likelihood of aggregation for insufficiently protected particles. With regard to DTT, this compound has a high affinity for gold surfaces because it is a dithiol moiety. Accordingly, DTT can plausibly displace long-chain sterically stabilizing thiol-based adsorbates from the AuNP surfaces in an exchange reaction and concomitantly fail to provide steric stabilization, which will also lead to particle aggregation.

In our study involving ionic strength, we compared colloidal stability for aqueous solutions with each of the adsorbate-capped AuNPs using 0.01, 0.1, 1, 10, and 100 mM concentrations of NaCl. In general, salt solutions are used for testing nanoparticles for biological studies because such solutions can reveal weaknesses for nanoparticle systems in vivo. Figure 7A shows the color changes for the solutions that include the AuNPs capped with MM, BM, MEM, and BEM at the NaCl concentrations listed above the first set of solutions. The AuNPs capped with OEG-deficient MM and BM exhibited the most dramatic color shifts after 48 h (i.e., from the pink color associated with a solution containing 0.01 mM NaCl to the light black/purple shades seen in the 10 mM NaCl solutions). These color changes for the solutions with the AuNPs protected by the mostly alkyl coatings were plausibly caused by aggregation of the AuNPs. However, the AuNPs capped with OEG-containing MEM or BEM showed only a slight change or no change in color even for the 100 mM NaCl solutions. Notably, AuNPs capped with adsorbates that contain OEG moieties in the termini of their alkyl chains have been observed to be stable in high ionic strength solutions.[51]

We also performed the stability test for our AuNPs in a variety of aqueous solutions of DTT as determined after 48 h at concentrations of 0.05, 0.5, 5, 50, and 500 mM (see Figure 7B). The solutions with the AuNPs capped with MM changed to a brownish color for the 5 mM sample and appeared to precipitate for the 500 mM solution. AuNPs capped with MEM showed a less intense light red color for the 50 mM solution but changed to a purple color for the 500 mM sample. In similar fashion to these results, there were no color changes for the AuNPs capped with BM until exposure with the 50 mM DTT solution. Importantly, AuNPs coated with BEM exhibited no color change for the 500 mM DTT solution, just a reduction in intensity. According to this visual analysis, the bidentate

DOI: 10.1021/acs.langmuir.6b01299
Langmuir 2016, 32, 7306–7315

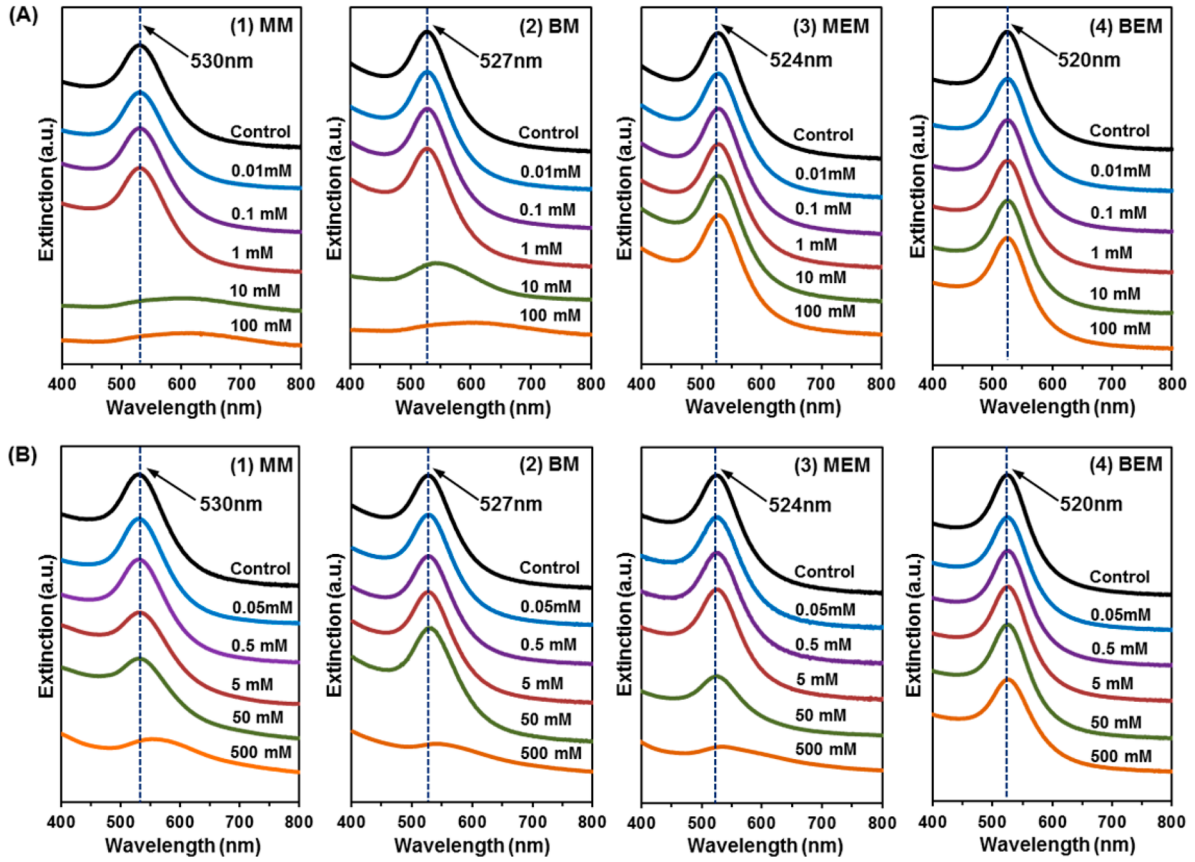

Figure 8. UV−vis spectra of aqueous solutions containing ∼15 nm AuNPs capped with either MM, BM, MEM, or BEM after 48 h for (A) the NaCl stability test and (B) the DTT stability test.

adsorbate-capped AuNPs were highly resistant to concentrated DTT solutions, as were both AuNP systems that included the OEG moieties in their tailgroups.

For a more quantitative analysis, Figure 8 shows the UV−vis spectra for both of the colloidal stability tests: NaCl and DTT. In plots 1 and 2 of Figure 8A, the AuNPs capped with MM and BM exhibit red-shifting, broadening, and decreasing intensity of the SPR band with increasing NaCl concentration. On the other hand, there appears to be little or no change for the spectra for the AuNPs capped with MEM and BEM, as shown in plots 3 and 4 of Figure 8A. These results are consistent with those shown in Figure 7 and can be rationalized by the fact that the OEG moieties impart water solubility for the AuNPs that is not impaired by the charged species in solution. For the DTT studies, the tests of the AuNPs capped with each of the adsorbates are shown in Figure 8B. In plots 1 and 3 of Figure 8B, the AuNPs capped with MM and MEM show decreasing intensity and peak broadening as the concentration of DTT was increased. The same trend occurs for the BM-capped AuNPs, but this feature is apparent only for the most concentrated DTT solution. Notably, the spectra of the BEM-capped AuNPs were constant even for the 500 mM DTT solution. Based on these results, it appears that the colloidal stability of the AuNPs in aqueous solution can best be enhanced by increasing the number of coordinating bonds to the surface of the AuNPs (i.e., using multidentate adsorbates) in combination with the incorporation of an OEG moiety at or near the termini of the adsorbate chains.

To help quantify the spectral data, Figures 9A and 9B were prepared to illustrate the SPR peak shifts as compared to the

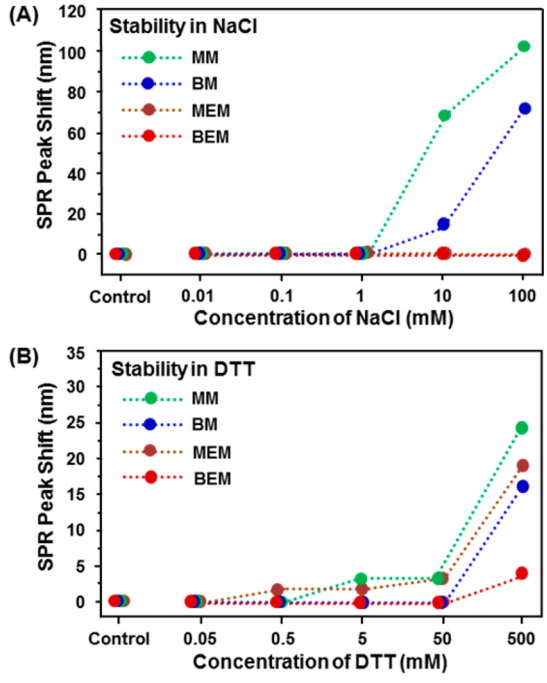

Figure 9. Profiles of the SPR peak shifts (as compared to the control sample) for ∼15 nm AuNPs functionalized with MM, BM, MEM, and BEM after 48 h of exposure (A) to 0.01, 0.1, 1, 10, and 100 mM aqueous solutions of NaCl and (B) to 0.05, 0.5, 5, 50, and 500 mM aqueous solutions of DTT. Dashed lines connecting data points are included as guides for the eye.

DOI: 10.1021/acs.langmuir.6b01299
Langmuir 2016, 32, 7306−7315

control samples using the peak position data obtained from the spectra in Figure 8 (see Tables S3 and S4). From the data for the NaCl study in Figure 9A, we observed that the AuNPs capped with adsorbates having no OEG moieties show high peak shift values because of low water solubility. From the data for the DTT study in Figure 9B, the bidentate adsorbate-capped AuNPs exhibit no change in their SPR peak positions until a concentration of 50 mM. However, at a DTT concentration of 500 mM, it is apparent that the AuNPs coated with BEM perform much better than the other AuNP systems capped with MM, BM, and MEM. According to these results, the AuNPs capped with BEM are remarkably more stable under high ionic conditions and when exposed to concentrated DTT solution.

CONCLUSIONS

A series of custom-designed maleimide-terminated alkanethioacetates were synthesized to provide a means of modifying gold nanostructures with maleimide attachment sites without the complexities typically encountered with thiol-based adsorbates. The resulting SAMs show that the new adsorbates afford well-defined monolayers on gold surfaces as characterized by XPS, PM-IRRAS, ellipsometry, and contact angle goniometry. For evaporated "flat" gold surfaces, the SAMs exhibited properties that depended on the deposition solvent used to form the SAMs, either EtOH or THF. All of the adsorbates yielded SAMs that exhibited higher packing densities when prepared in EtOH as compared to THF; however, the use of THF afforded SAMs with a higher percentage of bound thiolate. When used to functionalize AuNPs, colloidal stability tests revealed that the AuNPs capped with MEM and BEM exhibited high colloidal stability in NaCl solution, which was attributed to the OEG moieties in the tailgroups of the adsorbates. Additionally, BM- and BEM-coated AuNPs proved to be highly resistant to ligand exchange with DTT, which can be rationalized by the chelate effect for these bidentate adsorbates. Overall, the AuNPs capped with BEM exhibited better stability characteristics than the AuNPs capped with MM, BM, and MEM. This report should aid researchers in the design of nanoparticle-based systems for diagnostic and/or therapeutic applications that seek to employ the maleimide group as a conjugation tool.

ASSOCIATED CONTENT

Supporting Information

The Supporting Information is available free of charge on the ACS Publications website at DOI: 10.1021/acs.langmuir.6b01299.

Detailed descriptions of the synthetic procedures used to prepare the alkanethioacetate, along with the ^{1}H and ^{13}C NMR spectra for these compounds, the experimental procedures for preparing and characterizing the SAMs, and supplementary data (PDF)

AUTHOR INFORMATION

Corresponding Author

*E-mail: trlee@uh.edu (T.R.L.).

Notes

The authors declare no competing financial interest.

ACKNOWLEDGMENTS

We thank the National Science Foundation (CHE-1411265), the Robert A. Welch Foundation (Grant E-1320), and the Texas Center for Superconductivity at the University of Houston for generous support.

REFERENCES

(1) Love, J. C.; Estroff, L. A.; Kriebel, E. J.; Nuzzo, R. G.; Whitesides, G. M. Self-Assembled Monolayers of Thiolates on Metals as a Form of Nanotechnology. *Chem. Rev.* **2005**, *105*, 1103−1169.

(2) Ulman, A. Formation and Structure of Self-Assembled Monolayers. *Chem. Rev.* **1996**, *96*, 1533−1554.

(3) Bain, C. D.; Troughton, E. B.; Tao, Y. T.; Evall, J.; Whitesides, G. M.; Nuzzo, R. G. Fomration of Monolayer Films by the Spontaneous Assembly of Organic Thiols from Solution onto Gold. *J. Am. Chem. Soc.* **1989**, *111*, 321−335.

(4) Nuzzo, R. G.; Allara, D. L. Adsorption of Bifunctional Organic Disulfides on Gold Surfaces. *J. Am. Chem. Soc.* **1983**, *105*, 4481−4483.

(5) Béthencourt, M. I.; Srisombat, L.; Chinwangso, P.; Lee, T. R. SAMs on Gold Derived from the Direct Adsorption of Alkanethioacetates Are Inferior to Those Derived from the Direct Adsorption of Alkanethiols. *Langmuir* **2009**, *25*, 1265−1271.

(6) Lee, H. J.; Jamison, A. C.; Yuan, Y.; Li, C.-H.; Rittikulsittichai, S.; Rusakova, I.; Lee, T. R. Robust Carboxylic Acid-Terminated Organic Thin Films and Nanoparticle Protectants Generated from Bidentate Alkanethiols. *Langmuir* **2013**, *29*, 10432−10439.

(7) Lee, H. J.; Jamison, A. C.; Lee, T. R. Boc-Protected ω-Amino Alkanedithiols Provide Chemically and Thermally Stable Amine-Terminated Monolayers on Gold. *Langmuir* **2015**, *31*, 2136−2146.

(8) Zenasni, O.; Jamison, A. C.; Lee, T. R. The Impact of Fluorination on the Structure and Properties of Self-Assembled Monolayer Films. *Soft Matter* **2013**, *9*, 6356−6370.

(9) Houseman, B. T.; Gawalt, E. S.; Mrksich, M. Maleimide-Functionalized Self-Assembled Monolayers for the Preparation of Peptide and Carbohydrate Biochips. *Langmuir* **2003**, *19*, 1522−1531.

(10) Nair, D. P.; Podgorski, M.; Chatani, S.; Gong, T.; Xi, W.; Fenoli, C. R.; Bowman, C. N. The Thiol-Michael Addition Click Reaction: A Powerful and Widely Used Tool in Materials Chemistry. *Chem. Mater.* **2014**, *26*, 724−744.

(11) Mantovani, G.; Lecolley, F.; Tao, L.; Haddleton, D. M.; Clerx, J.; Cornelissen, J. J. L. M.; Velonia, K. Design and Synthesis of N-Maleimido-Functionalized Hydrophilic Polymers via Copper-Mediated Living Radical Polymerization: A Suitable Alternative to PEGylation Chemistry. *J. Am. Chem. Soc.* **2005**, *127*, 2966−2973.

(12) Tolstyka, Z. P.; Kopping, J. T.; Maynard, H. D. Straightforward Synthesis of Cysteine-Reactive Telechelic Polystyrene. *Macromolecules* **2008**, *41*, 599−606.

(13) Shakiba, A.; Jamison, A. C.; Lee, T. R. Poly(L-lysine) Interfaces via Dual Click Reactions on Surface-Bound Custom-Designed Dithiol Adsorbates. *Langmuir* **2015**, *31*, 6154−6163.

(14) Kuhn, S. J.; Finch, S. K.; Hallahan, D. E.; Giorgio, T. D. Proteolytic Surface Functionalization Enhances in Vitro Magnetic Nanoparticle Mobility through Extracellular Matrix. *Nano Lett.* **2006**, *6*, 306−312.

(15) Gindy, M. E.; Ji, S.; Hoye, T. R.; Panagiotopoulos, A. Z.; Prud'homme, R. K. Preparation of Poly(ethylene glycol) Protected Nanoparticles with Variable Bioconjugate Ligand Density. *Biomacromolecules* **2008**, *9*, 2705−2711.

(16) Zhu, J.; Chin, J.; Wangler, C.; Wangler, B.; Lennox, R. B.; Schirrmacher, R. Rapid ^{18}F-Labeling and Loading of PEGylated Gold Nanoparticles for in Vivo Applications. *Bioconjugate Chem.* **2014**, *25*, 1143−1150.

(17) Gobbo, P.; Workentin, M. S. Improved Methodology for the Preparation of Water-Soluble Maleimide-Functionalized Small Gold Nanoparticles. *Langmuir* **2012**, *28*, 12357−12363.

(18) Zhang, S.; Leem, G.; Srisombat, L.; Lee, T. R. Rationally Designed Ligands that Inhibit the Aggregation of Large Gold Nanoparticles in Solution. *J. Am. Chem. Soc.* **2008**, *130*, 113−120.

(19) Li, N.; Zhao, P.; Salmon, L.; Ruiz, J.; Zabawa, M.; Hosmane, N. S.; Astruc, D. "Click" Star-Shaped and Dendritic PEGylated Gold Nanoparticle Carborane Assemblies. *Inorg. Chem.* **2013**, *52*, 11146−11155.

DOI: 10.1021/acs.langmuir.6b01299
Langmuir 2016, 32, 7306−7315

(20) Brennan, J. L.; Hatzakis, N. S.; Tshikhudo, T. R.; Dirvianskyte, N.; Razumas, V.; Patkar, S.; Vind, J.; Svendsen, A.; Nolte, R. J. M.; Rowan, A. E.; Brust, M. Bionanoconjugation via Click Chemistry: The Creation of Functional Hybrids of Lipases and Gold Nanoparticles. *Bioconjugate Chem.* **2006**, *17*, 1373−1375.
(21) Sutton, H. C.; Winterbourn, C. C. On the Participation of Higher Oxidation States of Iron and Copper in Fenton Reactions. *Free Radical Biol. Med.* **1989**, *6*, 53−60.
(22) Bernardin, A.; Cazet, A.; Guyon, L.; Delannoy, P.; Vinet, F.; Bonnaffé, D.; Texier, I. Copper-Free Click Chemistry for Highly Luminescent Quantum Dot Conjugates: Application to in Vivo Metabolic Imaging. *Bioconjugate Chem.* **2010**, *21*, 583−588.
(23) Gobbo, P.; Novoa, S.; Biesinger, M. C.; Workentin, M. S. Interfacial Strain-promoted Alkyne−azide Cycloaddition (I-SPAAC) for the Synthesis of Nanomaterial Hybrids. *Chem. Commun.* **2013**, *49*, 3982−3984.
(24) Béthencourt, M. I.; Barriet, D.; Frangi, N. M.; Lee, T. R. Model Glycol-Terminated Surfaces for Adhesion Resistance. *J. Adhes.* **2005**, *81*, 1031−1048.
(25) Yang, Y. W.; Fan, L. J. High-Resolution XPS Study of Decanethiol on Au(111): Single Sulfur-Gold Bonding Interaction. *Langmuir* **2002**, *18*, 1157−1164.
(26) Castner, D. G. X-ray Photoelectron Spectroscopy Sulfur 2p Study of Organic Thiol and Disulfide Binding Interactions with Gold Surfaces. *Langmuir* **1996**, *12*, 5083−5086.
(27) Wenzler, L. A.; Moyes, G. L.; Raikar, G. N.; Hansen, R. L.; Harris, J. M.; Beebe, T. P., Jr. Measurements of Single-Molecule Bond-Rupture Forces between Self-Assembled Monolayers of Organosilanes with the Atomic Force Microscope. *Langmuir* **1997**, *13*, 3761−3768.
(28) Heeg, J.; Schubert, U.; Kuchenmeister, F. Mixed Self-Assembled Monolayers of Terminally Functionalized Thiols at Gold Surfaces Characterized by Angle Resolved X-Ray Photoelectron Spectroscopy (ARXPS) Studies. *Fresenius' J. Anal. Chem.* **1999**, *365*, 272−276.
(29) Lee, H. J.; Jamison, A. C.; Lee, T. R. Entropy-Driven Conformational Control of α,ω-Difunctional Bidentate-Dithiol Azo-Based Adsorbates Enables the Fabrication of Thermally Stable Surface-Grafted Polymer Films. *ACS Appl. Mater. Interfaces* **2016**, *8*, 15691−15699.
(30) Ishida, T.; Nishida, N.; Tsuneda, S.; Hara, M.; Sasabe, H.; Knoll, W. Alkyl Chain Length Effect on Growth Kinetics of *n*-Alkanethiol Self-Assembled Monolayers on Gold Studied by X-Ray Photoelectron Spectroscopy. *Jpn. J. Appl. Phys.* **1996**, *35*, 1710−1713.
(31) Ishida, T.; Hara, M.; Kojima, I.; Tsuneda, S.; Nishida, N.; Sasabe, H.; Knoll, W. High Resolution X-ray Photoelectron Spectroscopy Measurements of Octadecanethiol Self-Assembled Monolayers on Au(111). *Langmuir* **1998**, *14*, 2092−2096.
(32) Montague, M.; Ducker, R. E.; Chong, K. S. L.; Manning, R. J.; Rutten, R. J. M.; Davies, M. C.; Leggett, G. L. Fabrication of Biomolecular Nanostructures by Scanning Near-Field Photolithography of Oligo(ethylene glycol)-Terminated Self-Assembled Monolayers. *Langmuir* **2007**, *23*, 7328−7337.
(33) Wang, Y.; Cai, J.; Rauscher, H.; Behm, R. J.; Goedel, W. A. Maleimido-Terminated Self-Assembled Monolayers. *Chem. - Eur. J.* **2005**, *11*, 3968−3978.
(34) Harder, P.; Grunze, M.; Dahint, R.; Whitesides, G. M.; Laibinis, P. E. Molecular Conformation in Oligo(ethylene glycol)-Terminated Self-Assembled Monolayers on Gold and Silver Surfaces Determines Their Ability To Resist Protein Adsorption. *J. Phys. Chem. B* **1998**, *102*, 426−436.
(35) Li, L.; Chen, S.; Zheng, J.; Ratner, B. D.; Jiang, S. Protein Adsorption on Oiligo(ethylene glycol)-Terminated Alkanethiolate Self-Assembled Monolayers: The Molecular Basis for Nonfouling Behavior. *J. Phys. Chem. B* **2005**, *109*, 2934−2941.
(36) Rittikulsittichai, S.; Jamison, A. C.; Lee, T. R. Self-Assembled Monolayers Derived from Alkoxyphenylethanethiols Having One, Two, and Three Pendant Chains. *Langmuir* **2011**, *27*, 9920−9927.
(37) Perry, S. S.; Somorjai, G. A. Characterization of Organic Surfaces. *Anal. Chem.* **1994**, *66*, 403−415.
(38) Barriet, D.; Yam, C. M.; Shmakova, O. E.; Jamison, A. C.; Lee, T. R. 4-Mercaptophenylboronic Acid SAMs on Gold: Comparison with SAMs Derived from Thiophenol, 4-Mercaptophenol, and 4-Mercaptobenzoic Acid. *Langmuir* **2007**, *23*, 8866−8875.
(39) Porter, M. D.; Bright, T. B.; Allara, D. L.; Chidsey, C. E. D. Spontaneously Organized Molecular Assemblies. 4. Structural Characterization of *n*-Alkyl Thiol Monolayers on Gold by Optical Ellipsometry, Infrared Spectroscopy, and Electrochemistry. *J. Am. Chem. Soc.* **1987**, *109*, 3559−3568.
(40) Mak, L. H.; Sadeghi, S. J.; Fantuzzi, A.; Gilardi, G. Control of Human Cytochrome P450 2E1 Electrocatalytic Response as a Result of Unique Orientation on Gold Electrodes. *Anal. Chem.* **2010**, *82*, 5357−5362.
(41) Park, J. S.; Vo, A. N.; Barriet, D.; Shon, Y.-S.; Lee, T. R. Systematic Control of the Packing Density of Self-Assembled Monolayers Using Bidentate and Tridentate Chelating Alkanethiols. *Langmuir* **2005**, *21*, 2902−2911.
(42) Vaidya, A. A.; Norton, M. L. DNA Attachment Chemistry at the Flexible Silicon Elastomer Surface: Toward Disposable Microarrays. *Langmuir* **2004**, *20*, 11100−11107.
(43) Yıldırım, A.; Atmaca, U.; Keskin, A.; Topal, M.; Çelik, M.; Gülçin, I.; Supuran, C. T. N-Acylsulfonamides strongly inhibit human carbonic anhydrase isoenzymes I and II. *Bioorg. Med. Chem.* **2015**, *23*, 2598−2605.
(44) Weissman, M. R.; Winger, K. T.; Ghiassian, S.; Gobbo, P.; Workentin, M. S. Insights on the Application of the Retro Michael-Type Addition on Maleimide-Functionalized Gold Nanoparticles in Biology and Nanomedicine. *Bioconjugate Chem.* **2016**, *27*, 586−593.
(45) Oh, E. K.; Susumu, K.; Mäkinen, A. J.; Deschamps, J. R.; Huston, A. L.; Medintz, I. L. Colloidal Stability of Gold Nanoparticles Coated with Multithiol-Poly(ethylene glycol) Ligands: Importance of Structural Constraints of the Sulfur Anchoring Groups. *J. Phys. Chem. C* **2013**, *117*, 18947−18956.
(46) Underwood, S.; Mulvaney, P. Effect of the Solution Refractive Index on the Color of Gold Colloids. *Langmuir* **1994**, *10*, 3427−343.
(47) Wiesner, J.; Wokaun, A. Anisotropic Gold Colloid. Preparation, Characterization, and Optical Properties. *Chem. Phys. Lett.* **1989**, *157*, 569−575.
(48) Srisombat, L.−O.; Park, J. S.; Zhang, S.; Lee, T. R. Preparation, Characterization, and Chemical Stability of Gold Nanoparticles Coated with Mono-, Bis-, and Tris-Chelating Alkanethiols. *Langmuir* **2008**, *24*, 7750−7754.
(49) Ghosh, S. K.; Nath, S.; Kundu, S.; Esumi, K.; Pal, T. Solvent and Ligand Effects on the Localized Surface Plasmon Resonance (LSPR) of Gold Colloids. *J. Phys. Chem. B* **2004**, *108*, 13963−13971.
(50) Stewart, M. H.; Susumu, K.; Mei, B. C.; Medintz, I. L.; Delehanty, J. B.; Blanco-Canosa, J. B.; Dawson, P. E.; Mattoussi, H. Multidentate Poly(ethylene glycol) Ligands Provide Colloidal Stability to Semiconductor and Metallic Nanocrystals in Extreme Conditions. *J. Am. Chem. Soc.* **2010**, *132*, 9804−9813.
(51) Oh, E. K.; Susumu, K.; Goswami, R.; Mattoussi, H. One-Phase Synthesis of Water-Soluble Gold Nanoparticles with Control over Size and Surface Functionalities. *Langmuir* **2010**, *26*, 7604−7613.

DOI: 10.1021/acs.langmuir.6b01299
Langmuir 2016, 32, 7306−7315